

Probing nuclear properties and neutrino physics with current and future CE ν NS experiments

R. R. Rossi,^{1,*} G. Sanchez Garcia^{2,†} and M. Tórtola^{2,‡}

¹*Instituto de Física Gleb Wataghin, Universidade Estadual de Campinas, 13083-859, Campinas SP, Brazil*

²*Instituto de Física Corpuscular, CSIC-Universitat de València, Paterna 46980, Spain and Departament de Física Teòrica, Universitat de València, C/Catedrático José Beltrán 2, Paterna 46980, Spain*



(Received 4 December 2023; accepted 8 May 2024; published 30 May 2024)

The recent observation of coherent elastic neutrino-nucleus scattering (CE ν NS) with neutrinos from pion decay at rest (π -DAR) sources by the COHERENT Collaboration has raised interest in this process in the search for new physics. Unfortunately, current uncertainties in the determination of nuclear parameters relevant to those processes can hide new physics effects. This is not the case for processes involving lower-energy neutrino sources such as nuclear reactors. Note, however, that a CE ν NS measurement with reactor neutrinos depends largely on a (still-missing) precise determination of the quenching factor at very low energies, making its observation more challenging. In the upcoming years, once this signal is confirmed, a combined analysis of π -DAR and reactor CE ν NS experiments will be very useful to probe particle and nuclear physics, with a reduced dependence on nuclear uncertainties. In this work, we explore this idea by simultaneously testing the sensitivity of current and future CE ν NS experiments to neutrino nonstandard interactions (NSIs) and the neutron root mean square (rms) radius, considering different neutrino sources as well as several detection materials. We show how the interplay between future reactor and accelerator CE ν NS experiments can help to get robust constraints on the neutron rms and to break degeneracies between the NSI parameters. Our forecast could be used as a guide to optimize the experimental sensitivity to the parameters under study.

DOI: [10.1103/PhysRevD.109.095044](https://doi.org/10.1103/PhysRevD.109.095044)

I. INTRODUCTION

The process of coherent elastic neutrino-nucleus scattering (CE ν NS) was theoretically proposed more than 40 years ago [1]. In this process, a relatively low-energy neutrino interacts with a nucleus as a whole, and, as a result of the interaction, the nucleus acquires a kinetic recoil energy that can be measured. Given its low-energy signal, CE ν NS was not observed until 2017, when the COHERENT Collaboration reported its first experimental measurement by using neutrinos from the Spallation Neutron Source (SNS) and a cesium iodide (CsI) detector [2] at Oak Ridge National Laboratory. A second measurement was performed by the same collaboration in 2020 [3], this time by using a liquid argon (LAr) detector, and a more recent

dataset from the CsI detector was also released in 2021 [4]. Since then, CE ν NS has been widely used to test Standard Model (SM) parameters [5,6], to study nuclear physics parameters through the neutron root mean square (rms) radius [7,8], as well as to constrain new physics scenarios. These include neutrino nonstandard interactions (NSIs) [9–13], neutrino electromagnetic properties [14–17], neutrino generalized interactions [18–20], CP -violating effects [21], light mediators [22–24], sterile neutrinos [25,26], and dark fermion production [27], among many other scenarios. A recent combined analysis of COHERENT CsI and LAr data can be found in Ref. [28].

The coherent character of CE ν NS comes from the fact that, for energies up to some tens of MeV, the contribution to the cross section from the neutrons inside the nucleus adds up coherently, giving as a result a characteristic quadratic dependence on the number of neutrons of the target material. Because of the incoming neutrino energy range needed for coherency, neutrinos from pion decay at rest (π -DAR) sources are suitable to study CE ν NS. This is the case of the COHERENT Collaboration, which uses neutrinos produced at the SNS [29]. In addition, many other collaborations aim to measure CE ν NS from different π -DAR sources in the following years, such as the

*rossi@ifi.unicamp.br

†gsanchez@ific.uv.es

‡mariam@ific.uv.es

Published by the American Physical Society under the terms of the Creative Commons Attribution 4.0 International license. Further distribution of this work must maintain attribution to the author(s) and the published article's title, journal citation, and DOI. Funded by SCOAP³.

Coherent CAPTAIN-Mills experiment [30], as well as the experimental proposal at the future European Spallation Source (ESS) [31].

After the two successful measurements of CE ν NS by COHERENT, there has been a wide interest from the community on measuring CE ν NS by using different target materials and neutrino sources. For instance, using various materials can help to unambiguously corroborate the cross section's quadratic dependence on the number of neutrons of the target material. In fact, the complete COHERENT program includes detectors using different technologies such as Ge and NaI [32], as well as a proposed cryogenic CsI detector [33] at the SNS. As an alternative, the feasibility of using different isotopes of the same material to test the CE ν NS cross section has also been proposed in [34]. This approach can also be useful in the searches for new physics with CE ν NS. It has been shown, for example, that degeneracies in the determination of neutrino NSIs with matter can be lifted when combining CE ν NS results from different detectors [35]. As for practical purposes, the applicability of CE ν NS for reactor monitoring has also been studied [36].

Likewise, the interest in measuring CE ν NS from different neutrino sources has been increasing throughout the years. Indeed, very low thresholds in dark matter (DM) detectors will soon become sensitive to CE ν NS from solar neutrinos as part of their backgrounds. However, the most promising channel for CE ν NS detection through new neutrino sources is that of reactor neutrinos. These neutrinos are in a lower energy regime than those coming from π -DAR sources, and, hence, their detection is significantly important. In the case of π -DAR neutrinos, the cross section is sensitive to the nuclear structure of the target material through the form factor. In contrast, for reactor neutrino energies, nuclear distribution effects do not play a significant role, and so they are negligible (see Sec. III). This feature can be exploited to obtain complementary measurements that can help to study new physics effects without the uncertainties that come from nuclear effects.

Regarding the current status of CE ν NS searches using reactor neutrinos, suggestive evidence of a positive signal has been reported in [37]. Note, however, that its interpretation is highly dependent on quenching factor measurements. Beyond this result, many experimental efforts are currently under development with the aim of measuring CE ν NS from reactor neutrinos, as is the case of experiments like CONUS [38], ν GeN [39], CONNIE [40], and Red-100 [41], among many others. Then, a detailed forecast of the complementarity between current and future experiments of different neutrino sources is needed. In this work, we explore how the combination of CE ν NS experiments that use neutrinos produced from different sources could help us to constrain both NSIs and nuclear parameters. This kind of analysis was first explored in [42] for a single flavor-conserving NSI parameter. Here, we extend

the analysis to both nonuniversal and flavor-changing NSIs. In the case of π -DAR sources, we first make use of the latest data from the COHERENT CsI detector. In addition, we explore the expected sensitivity to the same parameters of two future π -DAR source experiments: a Ge detector located at the SNS and a proposed Xe detector at the future ESS. As for reactor neutrinos, we explore their near-future expected sensitivity to NSIs by considering the detector characteristics and background models of a CONUS-like [38] and a ν GeN-like experiment [39], each under a different quenching factor (QF) assumption, since the observation of CE ν NS for reactor neutrinos largely depends on this quantity. With this approach, our estimation of the sensitivity of future CE ν NS experiments will be as realistic as possible.

The remainder of this paper is organized as follows. In Sec. II, we discuss the theoretical features of CE ν NS, the role of the rms radius, and the general framework of NSIs. In Sec. III, we describe in detail the different neutrino sources considered in this work as well as the characteristics of the analyzed neutrino detectors. In Sec. IV, we discuss the analysis procedure followed to obtain the sensitivities on the nuclear physics and new physics scenarios investigated, with the corresponding results presented in Sec. V. Finally, we draw our conclusions in Sec. VI.

II. THEORETICAL FRAMEWORK

A. Coherent elastic neutrino-nucleus scattering

Within the SM, the CE ν NS cross section is given by [1]

$$\left(\frac{d\sigma}{dT}\right)_{\text{SM}} = \frac{G_F^2 M}{\pi} \left(1 - \frac{MT}{2E_\nu^2}\right) (Q_W^V)^2, \quad (1)$$

where G_F is the Fermi constant, M is the mass of the target material, T is the nuclear recoil energy, E_ν is the energy of the incoming neutrino, and Q_W^V is the weak charge, given by

$$(Q_W^V)^2 = (ZF_Z(q^2)g_V^p + NF_N(q^2)g_V^n)^2, \quad (2)$$

with $g_V^p = 1/2 - 2\sin^2\theta_W$ and $g_V^n = -1/2$ the coupling constants defined in the SM and θ_W the weak mixing angle. Notice that, within the SM, the CE ν NS cross section is flavor independent, with small corrections that have been studied in [43] but that are not relevant for current experimental sensitivities. The functions $F_Z(q^2)$ and $F_N(q^2)$ in Eq. (2) are called the proton and neutron form factors, respectively, and they describe the distribution of the corresponding protons and neutrons within the nucleus as a function of the momentum transfer, q . We can find different parametrizations to these form factors in the literature, including the symmetrized Fermi [44], the Helm [45], and the Klein-Nystrand [46] parametrizations.

Our results are independent of the parametrization, and we use the Klein-Nystrand one, which is given by

$$F_X(|\vec{q}|^2) = 3 \frac{j_1(|\vec{q}|R_X)}{|\vec{q}|R_X} \left(\frac{1}{1 + |\vec{q}|^2 a_k^2} \right), \quad (3)$$

with $X = Z, N$ standing for protons and neutrons, respectively. In this equation, j_1 is the spherical Bessel function of the order of 1, $a_k = 0.7$ fm, and each R_X satisfies [47]

$$R_Z^2 = \frac{5}{3} (R_p^2 - 6a_k^2) \quad (4)$$

and

$$R_N^2 = \frac{5}{3} (R_n^2 - 6a_k^2), \quad (5)$$

with R_p and R_n the proton and neutron rms radius, respectively. Thanks to the electromagnetic coupling of protons, there are many experimental measurements of the parameter R_p for different materials, with experimental precision of $\mathcal{O}(10^{-2}$ fm) and even $\mathcal{O}(10^{-3}$ fm) for some nuclei [48]. In contrast, the neutron rms radius is more difficult to determine, and, therefore, it is known only for a few nuclei [49]. Theoretical inputs for the neutron rms radius exist for a variety of nuclei like ^{40}Ar [50], among other nuclei relevant for CE ν NS detection [51]. These predictions, derived, for instance, from shell models, strongly constrain the neutron rms radius, based on predictions of the nuclear skin, $R_n - R_p$, with an estimated theoretical uncertainty of $\mathcal{O}(10^{-3}$ fm), arising from the calculation of the weak form factors in Eq. (3) [43]. Note, however, that these uncertainties strongly rely on theoretical assumptions and, depending on the model, may increase to $\mathcal{O}(10^{-2}$ fm) [43]. A correct estimate of the uncertainty on the neutron rms radius is crucial, since it has a significant impact on the computation of the CE ν NS cross section.¹ On the experimental side, measurements of the neutron rms radius, determined through parity-violation electron scattering, currently exist for nuclei like ^{208}Pb [52] and ^{48}Ca [53]. Moreover, the neutron skin has been estimated from antiprotonic x-ray data for a few nuclei [49], with a precision of up to $\mathcal{O}(10^{-2}$ fm). Besides those results, as recently shown, the study of CE ν NS can be used to determine the neutron rms radius [7]. In particular, the neutron rms radius for CsI has been constrained using latest COHERENT data with an uncertainty of the order of $\mathcal{O}(10^{-1}$ fm) [5]. Larger statistics and better control of systematic uncertainties will allow one to

¹A complete discussion of the relevant theoretical uncertainties in the calculation of the CE ν NS cross section from effective field theories, accounting for radiative corrections, can be found in Ref. [43].

improve this uncertainty soon, enhancing the importance of a correct characterization of CE ν NS detectors.

B. Nonstandard interactions

The formalism of NSIs accounts for possible new physics at low energies in the lepton sector of the SM and may affect neutrino interactions in their production, propagation, or detection. Here, we focus on the case of NSIs at the detection point, which was first studied in [54]. In general, NSIs can be of either charged or neutral current character. For the case of neutral current NSIs, our topic of interest, the Lagrangian that needs to be added to the SM, parametrized in terms of the Fermi constant, is given by

$$\mathcal{L}_{\text{NC}}^{\text{NSI}} = -2\sqrt{2}G_F \sum_{\alpha,\beta} \varepsilon_{\alpha\beta}^{fC} (\bar{\nu}_\alpha \gamma^\mu P_L \nu_\beta) (\bar{f} \gamma_\mu P_C f), \quad (6)$$

where Greek characters run over the three neutrino flavors, $C = L, R$ stands for the chirality, and f represents any of the SM charged fermions. The NSI constants $\varepsilon_{\alpha\beta}^{fC}$ parametrize the new physics strength of interaction weighted by G_F . Then, we expect these interactions to be below $\mathcal{O}(1)$ so that they are subdominant with respect to the SM weak force. Since we are interested in the interaction of neutrinos with a nucleus, we will focus on the case where the fermions are the up and down quarks within the nucleus. Then, once NSIs are introduced for an incoming neutrino of flavor α , the weak charge defined in Eq. (2) is modified to [55]

$$\begin{aligned} (Q_{W,\alpha}^{V,\text{NSI}})^2 = & [ZF_Z(q^2)(g_V^p + 2\varepsilon_{\alpha\alpha}^{uV} + \varepsilon_{\alpha\alpha}^{dV}) \\ & + NF_N(q^2)(g_V^n + \varepsilon_{\alpha\alpha}^{uV} + 2\varepsilon_{\alpha\alpha}^{dV})]^2 \\ & + \sum_{\beta \neq \alpha} |ZF_Z(q^2)(2\varepsilon_{\alpha\beta}^{uV} + \varepsilon_{\alpha\beta}^{dV}) \\ & + NF_N(q^2)(\varepsilon_{\alpha\beta}^{uV} + 2\varepsilon_{\alpha\beta}^{dV})|^2, \end{aligned} \quad (7)$$

where we have defined the vector coupling constants as²

$$\varepsilon_{\alpha\beta}^{qV} = \varepsilon_{\alpha\beta}^{qR} + \varepsilon_{\alpha\beta}^{qL}. \quad (8)$$

In contrast to the SM, where the weak force is universal and flavor conserving, NSIs can be either nonuniversal ($\alpha = \beta$) or flavor changing ($\alpha \neq \beta$). For a general review on neutrino NSIs, we refer the reader to Ref. [56].

III. NEUTRINO SOURCES FOR CE ν NS

In this section, we briefly describe two neutrino sources that can be used for the study of CE ν NS: stopped pion neutrinos and reactor neutrinos. Although we focus on

²Axial contributions in CE ν NS interactions are expected to be of the order of $1/A$, and, hence, they are negligible for the nuclei of interest.

these sources, we would like to remind the reader that very low threshold DM experiments will be sensitive to the CE ν NS contribution from solar neutrinos. Besides discussing the relevant neutrino sources, in this work, we also discuss several potential detectors that could be used in future CE ν NS searches. Our working scenarios can be regarded as futuristic or optimized versions of current detectors, such as COHERENT, CONUS, or ν GeN.

A. π -DAR sources

Neutrinos from these sources are produced through the collision of high-energy proton beams with a large-density target material. Spallation sources represent a particular kind of π -DAR sources on which proton beams are delivered in pulses with a well-determined frequency. This feature plays an important role in the determination and characterization of backgrounds for CE ν NS experiments. Here, charged pions are produced as a by-product of the proton collision. Then, pions are thoroughly stopped, and they decay at rest, producing muon neutrinos. Since this is a two-body decay, these neutrinos, often referred to as *prompt* neutrinos, have a fixed energy, and the corresponding flux can be described with a delta function:

$$\frac{dN_{\nu_\mu}}{dE_\nu}(E_\nu) = \eta \delta\left(E_\nu - \frac{m_\pi^2 - m_\mu^2}{2m_\pi}\right). \quad (9)$$

Here, m_π is the mass of the pion, m_μ is the mass of the muon, and $\eta = rN_{\text{POT}}/4\pi L^2$ is a normalization factor that depends on the distance from the source to the detector, L , and on the number of protons on target, N_{POT} . The pion yield r gives the ratio of produced π^+ per POT and, hence, quantifies the number of neutrinos of each species produced for each POT. As pions decay, there is also a production of muons, which eventually also decay at rest, producing electron neutrinos and muon antineutrinos. Since this last decay is a three-body process, the energy of the released neutrinos, known as *delayed* neutrinos, is no longer fixed, and it is described by the following distributions:

$$\frac{dN_{\bar{\nu}_\mu}}{dE_\nu}(E_\nu) = \eta \frac{64E_\nu^2}{m_\mu^3} \left(\frac{3}{4} - \frac{E_\nu}{m_\mu}\right), \quad (10)$$

$$\frac{dN_{\nu_e}}{dE_\nu}(E_\nu) = \eta \frac{192E_\nu^2}{m_\mu^3} \left(\frac{1}{2} - \frac{E_\nu}{m_\mu}\right), \quad (11)$$

where η is the same normalization factor defined above. Then, the total flux at π -DAR sources will be the sum of the three neutrino contributions in Eqs. (9)–(11). Once the cross section is known, the number of events for each neutrino flux component at a CE ν NS experiment can be computed as

$$N_{i,\alpha}^{\text{CE}\nu\text{NS}} = \mathcal{N} \int_{T_i}^{T_{i+1}} dT \epsilon(T) \int_0^{T'^{\text{max}}} dT' G(T, T') \times \int_{E_\nu^{\text{min}}(T')}^{E_\nu^{\text{max}}} dE_\nu \frac{dN_{\nu_\alpha}}{dE_\nu}(E_\nu) \frac{d\sigma}{dT'}(E_\nu, T'), \quad (12)$$

where i corresponds to the i th energy bin and \mathcal{N} is the number of targets inside the material. For a π -DAR experiment, $\mathcal{N} = N_A m_{\text{det}}/M_{\text{mol}}$, with N_A the Avogadro number, m_{det} the mass of the detector, and M_{mol} the molar mass of the material. The limits on the integral over E_ν are such that $E_\nu^{\text{min}} = \sqrt{MT'}/2$, while E_ν^{max} corresponds to the maximum energy for the incoming neutrinos, which for π -DAR sources is approximately 52.8 MeV. The resolution of the detector is accounted for by using the smearing function $G(T, T')$, which depends on the true recoil energy of the nucleus, T' , and the reconstructed energy, T . In addition, Eq. (12) includes the efficiency of the detector $\epsilon(T)$. The total number of events for an energy bin i is given by the sum over the three neutrino flux components:

$$N_i^{\text{CE}\nu\text{NS}} = \sum_\alpha N_{i,\alpha}^{\text{CE}\nu\text{NS}}. \quad (13)$$

In some cases, timing distributions for the measured CE ν NS events are provided by the experiment. Accounting for this information when necessary, the number of events associated to an energy bin i and a timing bin j can be calculated as

$$N_{ij}^{\text{CE}\nu\text{NS}} = \sum_\alpha N_{i,\alpha}^{\text{CE}\nu\text{NS}} \int_{t_j}^{t_{j+1}} f_\alpha(t) \epsilon_t(t) dt, \quad (14)$$

where $f_\alpha(t)$ is the flavor-dependent timing distribution and $\epsilon_t(t)$ is the timing efficiency. In this work, we consider the latest dataset of the COHERENT CsI detector, as well as two future data samples involving π -DAR sources. For the latter, we simulate future results to be obtained by an undergoing Ge detector from the COHERENT Collaboration at the SNS, and we analyze the sensitivity of a proposed Xe-based detector at the still-under-construction ESS.

1. COHERENT CsI detector at the SNS

In 2021, the COHERENT Collaboration reported an updated data set of the CsI detector used to measure CE ν NS [4]. The CsI detector was located at 19.3 m from the neutrino source, and, for the running time of the experiment, the collaboration reported a value of $N_{\text{POT}} = 3.198 \times 10^{23}$, with a number of neutrinos per flavor of $r = 0.0848$ [4]. These parameters are summarized in Table I and allow us to compute the total neutrino flux expected at the experiment. The smearing function $G(T, T')$, as well as the efficiency shape for the detector, is provided by the collaboration in supplemental material in

TABLE I. Relevant parameters for the simulation of the CE ν NS signal at π -DAR source experiments.

Experiment	Mass (kg)	Distance (m)	r	$N_{\text{POT}} (\times 10^{23})$	$T_{Th} (\text{keV}_{nr})$
CsI	14.3	19.3	0.0848	3.198	4.18
Ge	16	22	0.0848	2.24	2.272
Xe	20	20	0.3	2.8	0.9

Ref. [4] as a function of the number of photoelectrons (PEs) emitted by the scintillating material. These PEs result from the nuclear recoil energy and satisfy

$$\text{PE} = \text{LY} \times T_{ee}, \quad (15)$$

where LY is the light yield (13.35 PE/keV $_{ee}$ [2]) and T_{ee} is the electron-equivalent recoil energy. This quantity is related to the nuclear recoil energy T through

$$T_{ee} = \text{QF} \times T, \quad (16)$$

where QF is the *quenching factor*, defined as the fraction of kinetic recoil energy detected for the recoil of a heavy particle when compared to an incident electron of the same energy. For CsI, the electron-equivalent energy T_{ee} is a function of the nuclear recoil energy T , with a polynomial of order four dependence, which is provided in supplemental material in Ref. [4], and from which one can extract the QF at a given energy. Finally, the COHERENT Collaboration has also provided information on the timing distribution of CE ν NS events. Then, to compute the expected number of events due to CE ν NS, we use Eq. (14), with the timing shape taken from [57] and the corresponding efficiency from [4]. In Fig. 1, we show a projection of the obtained expected number of events in the nuclear energy recoil parameter space (left panel) and in the timing space (right panel). In the same figure, we also show the backgrounds as provided by the COHERENT Collaboration [4]. For the SNS, the reported dominant

contribution to them comes from steady state backgrounds (SSBs), which are those coming from natural sources such as cosmic rays. In addition, there is a minor contribution from beam-related neutrons (BRNs), produced as the result of the original proton collisions, and neutrino-induced neutrons (NINs), produced by charged and neutral current interactions of neutrinos with the lead shield surrounding the detector. The different bin widths in energy recoil in Fig. 1 are taken so that they match the PE width shown by the collaboration in Ref. [4].³

2. COHERENT Ge detector at the SNS

So far, the COHERENT Collaboration has reported CE ν NS measurements with two different detectors, one based on CsI, as discussed above, and another one using LAr. However, the complete experimental program of COHERENT includes two other detectors: COH-Ge-1 and COH-NaI-2 [32]. Here, we will focus on the expected sensitivity from COH-Ge-1, a germanium-based detector array that, when completed, will consist of eight p-type point-contact Ge detectors with an approximate mass of 2 kg each, giving a total mass of around 16 kg of detector material, located at 22 m from the neutrino source [32]. Regarding SNS characteristics, this facility currently operates at a proton beam energy of 1 GeV, with a power beam of 1.4 MW, although it is expected to be increased up to 2 MW in the near future. For our simulation, we consider this last value of the beam power, corresponding to $N_{\text{POT}} = 2.24 \times 10^{23}$ for one calendar year of SNS operations and to approximately 5000 h of data taking [32]. For the number of neutrinos per flavor released, we take the current reported value of $r = 0.0848$ [4]. Regarding the energy resolution of the detector, we consider a Gaussian smearing function with 85 keV $_{ee}$ FWHM, and we assume a conservative efficiency of 95%. A summary of all the parameters considered for the calculation of the number of events for this experiment is given in Table I. With all these considerations, we simulate the spectrum for one calendar year of SNS operations, as shown in the left panel in Fig. 2, where the bin size corresponds to 1 keV $_{ee}$ assuming a constant QF of 0.22. Besides the spectrum of CE ν NS events, we also include in the figure the three main expected sources of backgrounds: SSB and NIN + BRN. The distribution of background events, taken from [58],

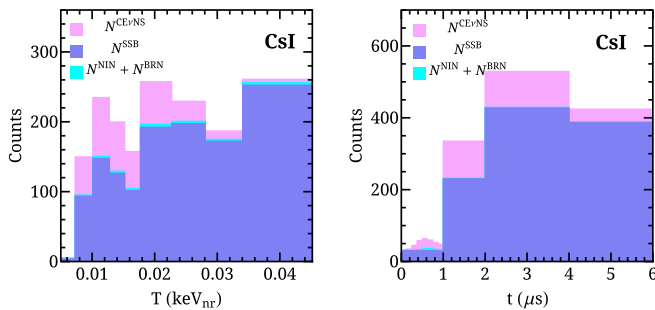


FIG. 1. Predicted number of CE ν NS events by the SM for the CsI detector used by the COHERENT Collaboration. The left panel shows the results in the recoil energy T , parameter space, while the right panel shows the distribution in time. Besides CE ν NS data (pink), the associated backgrounds are also indicated in the figure: SSB in purple and NIN + BRN in cyan.

³For more details of the binning distribution and background treatments, we refer the reader to Ref. [28].

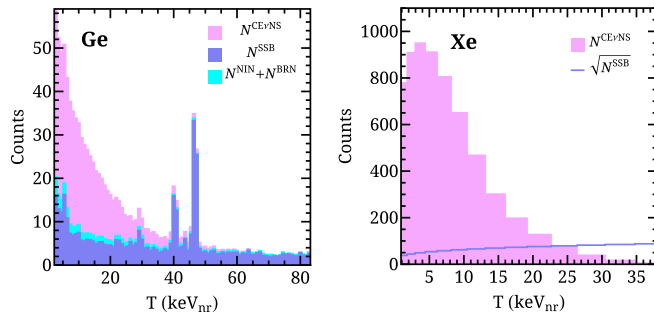


FIG. 2. Expected number of events after one year of data taking at the π -DAR source experiments under consideration. The left panel corresponds to the signal (CE ν NS + backgrounds) predicted for the Ge detector experimental setup, while the right panel presents the spectrum expected for the xenon detector at the ESS described in the text. For clarity, the blue line corresponds to the square root of the expected SSB backgrounds, denoted as $\sqrt{N^{\text{SSB}}}$.

shows that SSB constitutes the dominant contribution for backgrounds at the SNS.

3. Xenon detector at the ESS

Here, we will also analyze the expected sensitivity of a CE ν NS detector located at the future ESS. Even though this facility is still under construction, several experimental proposals are considering its particle physics potential [59], including the possibility of measuring CE ν NS with different detection materials. As a working example, we consider the case of a Xe-based detector with the same characteristics as proposed in [31] and summarized in Table I. One of the main advantages of using the ESS is its relatively large maximum beam energy of 2 GeV and its beam power of 5 MW, under which $r = 0.3$. This allows for having $N_{\text{POT}} = 2.8 \times 10^{23}$ in a calendar year of operation, which, as in the case of the SNS, corresponds to approximately 5000 h. Regarding backgrounds, we consider the model given in [31], according to which the contributions of BRN and NIN in this facility are expected to be negligible. However, one finds that the lower-frequency pulse of the ESS in comparison to the SNS slightly reduces the SSB background discrimination power of the experiment.⁴ The relevant parameters necessary to calculate the expected number of CE ν NS events are shown in Table I. For the detector, we considered a Gaussian smearing function and an efficiency of 80% following the prescription given in [31]. The obtained spectrum and modeled backgrounds are shown in the right panel in Fig. 2. Our result is consistent with the spectrum reported in Ref. [35], where they

⁴In the bins that represent the 80% of the CE ν NS signal for our experimental setups, the signal to background ratio lays between 1.77 and 2.93 for the Ge (SNS) detector and between 0.19 and 0.54 for the Xe (ESS) detector.

consider a three-year data taking for the same detector characteristics.

B. Reactor experiments

As discussed in the introduction, there is great interest within the community to pursue new CE ν NS measurements from neutrino sources other than π -DAR. Nuclear reactors can constitute a very interesting source for CE ν NS neutrino experiments. There, electron antineutrinos are emitted by the beta decay of neutron-rich elements produced in the chain reactions that take place inside the reactor. The main contribution to this neutrino flux comes from the decay of four elements with different average proportions, which depend on the characteristics of the nuclear reactor [60]. Here, we will assume ^{235}U : 0.56, ^{239}Pu : 0.31, ^{238}U : 0.07, and ^{241}Pu : 0.06. These fission fractions vary over time as the fuel inside the reactor burns, so one can consider an average value. For energies above 1.8 MeV, where kinematics allows the detection of reactor antineutrinos via inverse beta decay, the antineutrino spectrum can be modeled by the Huber-Mueller parametrization [61,62]

$$\lambda(E_\nu) = \sum_m f_m \exp \left[\sum_{k=1}^6 \alpha_{m,k} E_\nu^{k-1} \right], \quad (17)$$

where f_m are the fission fractions discussed above and the coefficients $\alpha_{m,k}$ are defined in Refs. [61,62]. Below the kinematic threshold for inverse beta decay, the antineutrino spectrum can be modeled as in Ref. [63]. However, for current detector thresholds regarding CE ν NS experiments, only neutrino energies above 2 MeV are relevant.⁵ The total number of events for a given reactor experiment is determined from Eq. (12), by substituting the π -DAR neutrino spectrum by the normalized reactor spectrum in Eq. (17) multiplied by the corresponding flux.

Following the description above, we have estimated the sensitivities of possible future CE ν NS searches at reactor neutrino experiments. The proposed experimental setups are based on the reported configuration for backgrounds, thresholds, and masses of the CONUS [38] and ν GeN [39] experiments. One of the main advantages of studying CE ν NS with reactor neutrinos is that, due to their energy, the expected signal is blind to the effects of the proton and neutron form factors. This is not the case for stopped pion neutrinos, where the role of form factors is relevant and can be confused with other new physics contributions to the CE ν NS cross section. Therefore, the combined analysis of CE ν NS experiments using π -DAR and reactor neutrino

⁵Assuming a QF of 0.22 (0.19) and a 200 keV $_{\text{ec}}$ threshold for a Ge detector, the associated nuclear recoil energy is $T \approx 0.90$ keV (1.05 keV), which requires a minimum neutrino energy of ≈ 5.5 MeV (5.9 MeV).

TABLE II. Different cases analyzed for the CONUS-like and ν GeN-like reactor experiments.

CONUS-like				ν GeN-like			
$d = 17 \text{ m}, \phi = 2.3 \times 10^{13} \text{ cm}^{-2} \text{ s}^{-1}$				$d = 11 \text{ m}, \phi = 4 \times 10^{13} \text{ cm}^{-2} \text{ s}^{-1}$			
Case	Time (yr)	Mass (kg)	ROI (keV _{ee})	Case	Time (yr)	Mass (kg)	ROI (keV _{ee})
1	1	4	[0.296, 0.446]	1	1	1.4	[0.32, 0.36]
2	1	16	[0.296, 0.446]	2	1	16	[0.32, 0.36]
3	1	4	[0.276, 0.446]	3	1	1.4	[0.30, 0.45]
4	1	16	[0.276, 0.446]	4	1	16	[0.28, 0.45]
5	1	4	[0.216, 0.446]	5	1	1.4	[0.24, 0.45]

sources can help disentangle the nuclear physics parameters from the potential signals of physics beyond the SM.

1. CONUS-like Ge detector

CONUS was a CE ν NS experiment having the reactor at the Brokdorf power plant as its neutrino source [64], with a thermal power of 3.9 GW and a total flux of 2.3×10^{13} antineutrinos per cm²/s for an average distance of 17 m from the detector to the reactor. The CONUS Collaboration has not observed a positive signal of CE ν NS but has reported upper limits to the associated cross section [38]. The upgrade of the detector to CONUS+ is currently under way [65]. Here, we study the sensitivity that a detector similar to CONUS can reach in a scenario where the measurement of CE ν NS is achieved. During its first two runs, CONUS used four high-purity p-type Ge detectors, each with an approximate mass of 1 kg. As reported in Ref. [38], each detector had different thresholds and regions of interest for data analysis. To study the future sensitivity of a CONUS-like experiment, we will assume four detectors with the same characteristics as the detector C1 in Ref. [38], for one year of data taking. This means that we assume 4 kg of total fiducial mass and a threshold of 0.296 keV_{ee}. A summary of the relevant parameters for the calculation of the total number of events is given in Table II (see Sec. VC). The background model for the analysis is taken from Ref. [38] and scaled to one year of data taking. Note that the dominant contribution to backgrounds comes from cosmic rays, and, then, it is not correlated with reactor backgrounds, which are negligible [66]. Note as well that the background spectrum is presented in bins of width 0.01 keV_{ee}. To convert this signal into the equivalent one in nuclear recoil energy, we assume an average QF of 0.19 in the region of interest. As for the smearing function, by following the prescription in [38], we assume a detector efficiency of 95% and a Gaussian smearing with 85 keV_{ee} FWHM. Under these assumptions, we get the distribution shown in the left panel in Fig. 3, where we have considered a ⁷²Ge detector. For reference, the yellow band in the figure indicates the region of interest for the C1 detector, conveniently chosen by the

collaboration to increase the efficiency and reduce backgrounds [38].

2. ν GeN-like Ge detector

As a second working example of reactor sources, we consider the characteristics of the ν GeN experiment [39]. As in the case of CONUS, a signal of CE ν NS has not been reported by the ν GeN Collaboration yet. Then, here we will analyze the potential sensitivity of the ν GeN-like experimental setup assuming a positive measurement can be achieved. Currently, the ν GeN experiment is located at the Kalinin nuclear power plant, with a thermal power of 3.1 GW and an impressive flux of 4×10^{13} antineutrinos per cm²/s for a detector located 11 m from the core of the reactor. The experiment consists of a p-type Ge detector with a current fiducial mass of 1.4 kg that can be further extended. As indicated in Ref. [39], the region of interest for this detector goes from 0.32 to 0.36 keV_{ee}. To convert those energies into nuclear recoil equivalent energies, we assume a constant QF of 0.20. A summary of the detector characteristics is given in Table II (see Sec. VC). Regarding the smearing, we assume a Gaussian distribution with 10.4 keV_{ee} FWHM, and we take

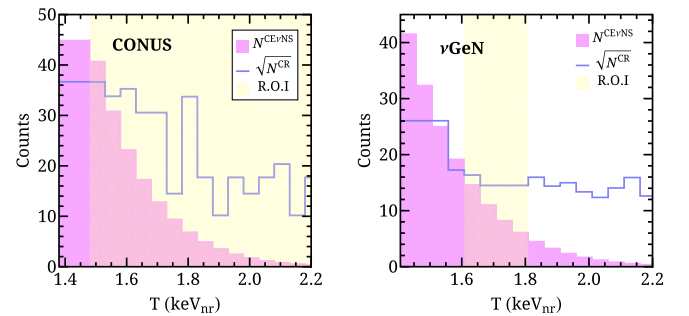


FIG. 3. Expected CE ν NS spectrum at reactor experiments. The left panel shows the expected signal at the considered CONUS-like experiment described in the text. The right panel shows the corresponding expected events for the ν GeN-like experiment. In both cases, the squared root of the cosmic ray backgrounds, N^{CR} , is shown in blue, and the experimental region of interest is indicated between yellow bands.

the efficiency from [39]. Under these assumptions, we simulate the expected event rate shown in the right panel in Fig. 3, where we also present the backgrounds taken from Ref. [39] and scaled to one-year data taking, again with a dominant contribution from cosmic rays. Yellow bands in the figure indicate the region of interest reported by the collaboration.

IV. ANALYSIS

Once we have presented the different experimental setups under consideration, we now describe the strategy used to test the neutron rms radius as well as to constrain NSI parameters. Our ultimate goal will be combining different neutrino sources to constrain these parameters when simultaneously studied. The procedure we follow is essentially based on Ref. [42], although here we consider additional NSI parameters and present our results with the up-to-date data from the CsI COHERENT detector. Besides, we consider more realistic scenarios of backgrounds and efficiencies regarding future experiments.

We first analyze the current data from the CsI detector at the SNS using the following Poissonian χ^2 function [28]:

$$\chi^2 = 2 \sum_{i,j} \left[N_{ij}^{\text{th}}(X) - N_{ij}^{\text{exp}} + N_{ij}^{\text{exp}} \ln \left(\frac{N_{ij}^{\text{exp}}}{N_{ij}^{\text{th}}(X)} \right) \right] + \sum_{m=1}^2 \frac{\alpha_m}{\sigma_{\alpha_m}^2} + \sum_{k=1}^3 \frac{\beta_k}{\sigma_{\beta_k}^2}, \quad (18)$$

with

$$N_{ij}^{\text{th}}(X) = (1 + \alpha_1) N_{ij}^{\text{CE}\nu\text{NS}}(X, \alpha_2, \alpha_3) + (1 + \beta_1) N_{ij}^{\text{SSB}} + (1 + \beta_2) N_{ij}^{\text{BRN}}(\alpha_3) + (1 + \beta_3) N_{ij}^{\text{NIN}}(\alpha_3). \quad (19)$$

Here, the i index runs over recoil energy bins, and the j index runs over the time bins, N_{ij}^{exp} being the measured number of events at each bin⁶ and $N_{ij}^{\text{th}}(X)$ the predicted total number of events, which includes CE ν NS interactions (as a function of a set of the parameters under test, X), as well as the contributions from SSB, BRN, and NIN background events, denoted as N_{ij}^{SSB} , N_{ij}^{BRN} , and N_{ij}^{NIN} , respectively. The parameters α_m and β_m in Eqs. (18) and (19) are nuisance parameters with respect to which we perform the minimization process, each with its associated systematic uncertainty σ_{α_m} and σ_{β_k} , which values are taken from [28]. The parameters indicated as α_m have an impact on the CE ν NS signal and background predictions, α_1 being solely associated with the flux normalization and QF. On the other hand, the parameter α_2 is introduced as in [28] to

account for the CE ν NS efficiency uncertainty and α_3 for the uncertainty in timing distribution, which also has an effect on the BRN and NIN background distributions. In addition, β_k parameters are introduced to account for background normalizations, with $k = 1, 2, 3$ for SSB, BRN, and NIN, respectively.

In the case of future experiments, we do not consider timing distribution, and we perform the analysis by minimizing the function

$$\chi^2 = 2 \sum_i \left[N_i^{\text{th}}(X) - N_i^{\text{exp}} + N_i^{\text{exp}} \ln \left(\frac{N_i^{\text{exp}}}{N_i^{\text{th}}(X)} \right) \right] + \frac{\alpha_1}{\sigma_{\alpha_1}^2} + \sum_k \frac{\beta_k}{\sigma_{\beta_k}^2} \quad (20)$$

with

$$N_i^{\text{th}}(X) = (1 + \alpha_1) N_i^{\text{CE}\nu\text{NS}}(X) + \sum_k (1 + \beta_k) N_i^{\text{bckg-}k}. \quad (21)$$

where the i index runs over recoil energy bins. In the previous equation, $N_i^{\text{th}}(X)$ is the theoretical number of events expected at each bin by considering the contribution from CE ν NS, $N_i^{\text{CE}\nu\text{NS}}(X)$, and the corresponding backgrounds $N_i^{\text{bckg-}k}$. The parameter α_1 has the same meaning as in Eq. (19), and the parameters β_k are associated with background normalizations. The nature and number of the different background contributions will be different depending on the experiment under analysis. In the case of a Ge detector at the SNS, we consider two nuisance parameters ($k = 1, 2$): one denoted as β_1 , associated to SSB events ($N_i^{\text{SSB}} \equiv N_i^{\text{bckg-}1}$), and another one, denoted as β_2 , for BRN + NIN events ($N_i^{\text{BRN+NIN}} \equiv N_i^{\text{bckg-}2}$). On the other hand, for the Xe detector at the ESS, we follow the procedure in Ref. [31], and we neglect the BRN + NIN contribution to the number of events. For reactors, we consider only one dominant contribution to backgrounds coming from cosmic ray muons ($N_i^{\text{CR}} \equiv N_i^{\text{bckg-}1}$) and, hence, one single nuisance parameter β_1 . For both neutrino source experiments, N_i^{exp} refers to the measured number of events, which, as we are considering future experiments, we will assume as the SM prediction plus background contributions as described in the previous section. Following this procedure, we will be able to estimate the sensitivity of a given experiment to the parameter under study through its impact on the CE ν NS predicted signal.

V. RESULTS

In this section, we present our main results for the sensitivity of the current and future discussed experiments to both the neutron rms radius and NSI parameters. We begin by studying the parameters individually, then we simultaneously study both parameters on π -DAR sources,

⁶See Ref. [67] and Appendix in Ref. [28].

which are sensitive to the neutron rms radius, and, finally, we combine the results of the two different sources.

A. Nuclear physics from π -DAR experiments

As discussed in the introduction, the process of $\text{CE}\nu\text{NS}$ is sensitive to the neutron rms radius of the target material through the form factor defined in Eq. (3). Experimentally, this parameter has been measured only for a few materials. For instance, the rms radius for ^{208}Pb and ^{48}Ca were determined from parity-violating processes at the Lead (Pb) Radius Experiment (PREX) [52,68] and Calcium Radius Experiment (CREX) [53] experiments, respectively. A precise determination of this parameter for the target materials considered here is of particular interest for neutrino physics. For instance, Ge detectors are used in the searches for neutrinoless double beta decay, and Xe detectors are also used in dark matter searches, where the $\text{CE}\nu\text{NS}$ signal may contribute to the so-called *neutrino floor*, an irreducible neutrino background for dark matter direct detection. To test the sensitivity of π -DAR experiments to the neutron rms radius, we consider the cross section introduced in Eq. (1), and we compute the number of events by varying the parameter R_n in Eq. (5) while keeping the proton rms radius R_p to a fixed value. An analysis involving the R_n parameter alone for CsI data has already been discussed in Ref. [28], so we start our discussion with the expectations for the future proposals introduced in Sec. III.

We first consider a ^{72}Ge detector at the SNS with the characteristics described in Sec. III for one calendar year of SNS operations and with $R_p = 4.06$ fm [48]. The results of the analysis are shown in the left panel in Fig. 4. For the analysis, we have considered a conservative systematic error uncertainty of $\sigma_{\alpha_1} = 10\%$. In addition, we considered the SSB and BRN + NIN backgrounds as discussed in Sec. III, with their corresponding uncertainties of $\sigma_{\beta_1} = 5\%$ and $\sigma_{\beta_2} = 25\%$, which were motivated by the current status of the CsI and LAr detectors used by the COHERENT Collaboration. The 90% CL expected sensitivity of the experiment is given by

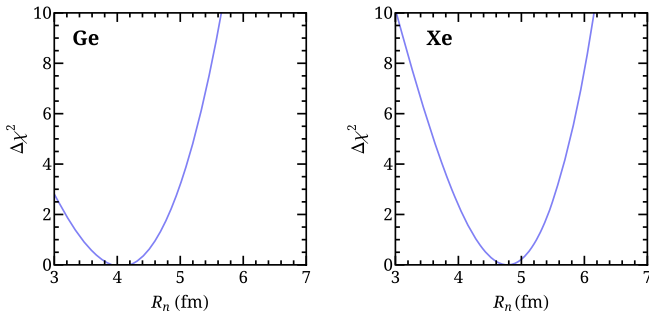


FIG. 4. Expected sensitivity of π -DAR experiments to the neutron rms radius. The left panel shows the results for a Ge detector at the SNS, and the right panel assumes a Xe detector located at the ESS. In both cases, one year of operations has been assumed.

$$3.0 \text{ fm} \leq R_n^{\text{Ge}} \leq 4.9 \text{ fm}. \quad (22)$$

As a second scenario, we study the expected sensitivity to the neutron rms radius of a Xe detector at the ESS with the characteristics described in Sec. III. Again, for the analysis, we vary the corresponding value of R_n while keeping the proton rms radius fixed to a value of $R_p = 4.73$ fm [48]. The result for one year of ESS operations is shown in the right panel in Fig. 4, where we have considered only the contribution to backgrounds from SSB as described before. Assuming the corresponding uncertainties as $\sigma_{\alpha_1} = 10\%$ and $\sigma_{\beta_1} = 1\%$ [31], we obtain the following expected sensitivity at 90% CL:

$$3.9 \text{ fm} \leq R_n^{\text{Xe}} \leq 5.5 \text{ fm}. \quad (23)$$

Notice that the two panels in Fig. 4 are not directly comparable, since we are working with different nuclei as target materials used for detection. However, we note that the constraints for the Xe detector are slightly better, as a consequence of the larger statistics expected for this detector, since the $\text{CE}\nu\text{NS}$ cross section effectively scales as N^2 .

B. NSIs from π -DAR experiments

We now turn our attention to the sensitivity of π -DAR source experiments to neutrino nonstandard interactions at the detection point for the same experimental setups considered above. To this end, we now calculate the predicted number of events using the cross section with the weak charge as given in Eq. (7) and assuming only one NSI parameter to be different from zero at a time. This scenario has been discussed in detail for the CsI detector in Ref. [28], and here we present the analysis for the future proposals introduced in Sec. III. The results for a ^{72}Ge detector at the SNS are presented in Fig. 5, where we show the expected $\Delta\chi^2$ profiles for nonuniversal (left panel) and

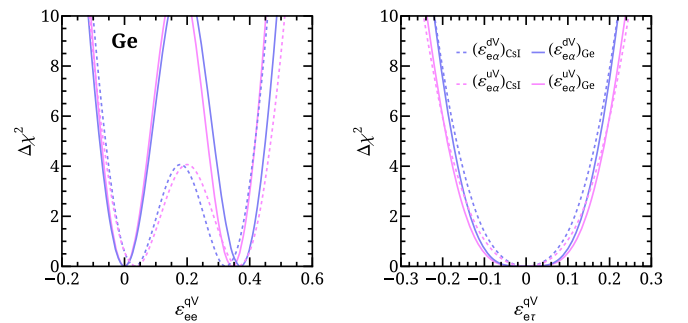


FIG. 5. Solid lines show the expected sensitivity of a Ge detector at the SNS to nonuniversal (left panel) and flavor-changing (right panel) NSI couplings with up (pink curves) and down (blue curves) quarks. Dashed lines (with the same color code) correspond to the current bounds obtained from the analysis of COHERENT CsI data [28].

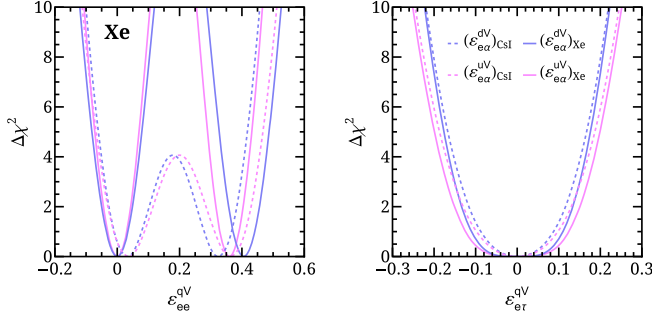


FIG. 6. Solid lines show the expected sensitivity of a Xe detector at the ESS to nonuniversal (left panel) and flavor-changing (right panel) NSI couplings with up (pink curves) and down (blue curves) quarks. Dashed lines (with the same color code) correspond to the current bounds obtained from the combined analysis of COHERENT data [28].

flavor-changing (right panel) neutrino NSIs with up (pink curves) and down (blue curves) quarks.

When compared to current bounds on NSIs from CEνNS (see the dashed lines in the plot), one sees that the expected constraints for nonuniversal NSIs are slightly better than the ones obtained from the analysis of COHERENT measurements [28], which is mainly driven by CsI data. For the case of nonuniversal NSIs in future experiments, we see a local minimum at $\varepsilon_{ee}^{qV} = 0$, corresponding to the SM solution, and a second minimum at $\varepsilon_{ee}^{uV} \approx 0.34$ and $\varepsilon_{ee}^{dV} \approx 0.37$. This is expected, since, for these values, the combination of the standard and nonstandard couplings mimics the SM prediction, as discussed in [35]. At 90% CL, we get the following expected sensitivity to nonuniversal NSIs:

$$-0.058 \leq \varepsilon_{ee}^{dV} \leq 0.060 \cup 0.310 \leq \varepsilon_{ee}^{dV} \leq 0.428, \quad (24)$$

$$-0.052 \leq \varepsilon_{ee}^{uV} \leq 0.055 \cup 0.288 \leq \varepsilon_{ee}^{uV} \leq 0.399. \quad (25)$$

Regarding flavor-changing NSI couplings, shown in the right panel in the same figure, there is only one minimum, corresponding to $\varepsilon_{e\tau}^{qV} = 0$. This result is also expected, since, in this case, there is no possible interference between the SM and the NSI contribution to the cross section, as seen from Eq. (7). The expected sensitivity at 90% CL is

$$|\varepsilon_{e\tau}^{dV}| \leq 0.145, \quad |\varepsilon_{e\tau}^{uV}| \leq 0.156. \quad (26)$$

Notice that, in this case, the proposed future experiment would not be able to improve the current bounds on flavor-changing NSIs for one year of data taking. However, in the next section, we will analyze the impact of combining these results with future reactor data.

For completeness, we show in Fig. 6 the corresponding results for a potential Xe detector located at the ESS. As before, the left panel in the figure shows the results for

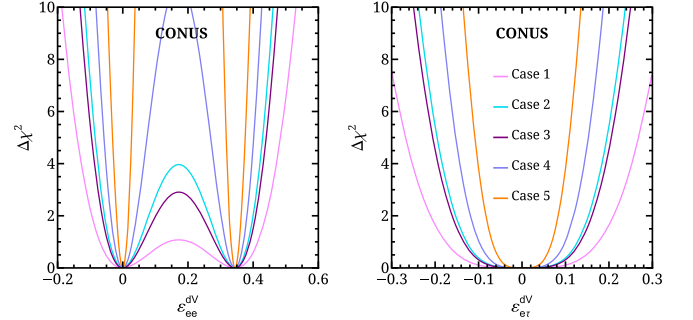


FIG. 7. Expected sensitivity of a CONUS-like detector to nonuniversal (left panel) and flavor-changing (right panel) NSI couplings with down quarks. The different configurations are defined in Table II, and the color code is the same for the two panels.

nonuniversal NSI couplings, while the right panel presents the case of flavor-changing NSIs. As in the previous case, we find two solutions for the nonuniversal NSI couplings ε_{ee}^{qV} , although here the non-SM local minimum is shifted with respect to the one obtained for the Ge detector in Fig. 5. This is because the position of this minimum depends on the ratio of protons to neutrons in the target material. The 90% CL expected sensitivity of this experimental setup to ε_{ee}^{qV} is given by

$$-0.058 \leq \varepsilon_{ee}^{dV} \leq 0.056 \cup 0.347 \leq \varepsilon_{ee}^{dV} \leq 0.465, \quad (27)$$

$$-0.052 \leq \varepsilon_{ee}^{uV} \leq 0.050 \cup 0.307 \leq \varepsilon_{ee}^{uV} \leq 0.411, \quad (28)$$

while for flavor-changing NSIs we obtain

$$|\varepsilon_{e\tau}^{dV}| \leq 0.145, \quad |\varepsilon_{e\tau}^{uV}| \leq 0.165. \quad (29)$$

C. NSIs from reactor experiments

As we have already discussed, reactor neutrinos are not sensitive to the nuclear information of the target material. Therefore, in this section, we will focus on only the expected sensitivity of reactor experiments to NSIs. We first consider a CONUS-like experiment with the background model and detector characteristics described in Sec. III. Following the same procedure as in the SNS case, we assume only one NSI parameter to be different from zero at a time. The results are shown in Fig. 7 for nonuniversal (left panel) and flavor-changing (right panel) NSIs.⁷ The pink lines (labeled as “case 1” in the figure) correspond to the CONUS reported characteristics regarding mass and threshold, as discussed in Sec. III. Since the

⁷For comparison, the 90% CL allowed interval on the non-universal NSI coupling, $\varepsilon_{ee}^{dV} \in (-0.096, 0.069) \cup (0.279, 0.437)$, has been obtained in Ref. [69] from the suggestive evidence of CEνNS from reactors reported in [37].

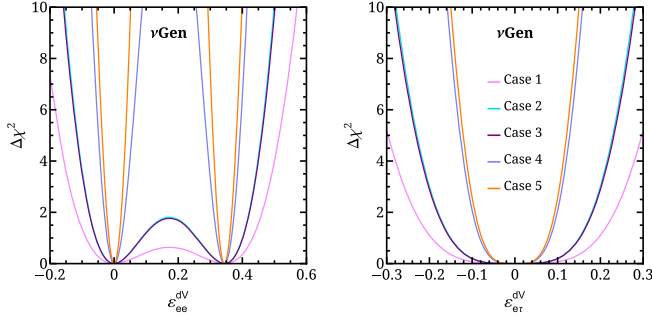


FIG. 8. The same as Fig. 10 for a νGeN -like detector for the experimental setups indicated in Table II. The color code is the same for the two panels.

results are qualitatively similar for up and down quark couplings (see Fig. 5), here we focus on the sensitivities to NSIs with down quarks, exploring as well the sensitivity of eventual future scenarios for a CONUS-like experiment. Thus, besides case 1, we consider four additional possibilities, allowing for larger detector masses and lower energy thresholds; see Table II.

Coming back to Fig. 7, the left panel shows that, for case 1, at 90% CL the coupling ϵ_{ee}^{dV} is constrained to a single interval that contains the two minima discussed before. By lowering the threshold, as in case 3, the sensitivity is improved and the degeneracy breaks at 90% CL. This enhanced sensitivity can also be obtained by increasing the mass of the detector from the original CONUS configuration of 4 kg to 16 kg while keeping the original threshold; see case 2. Under these conditions, the degeneracy in the determination of the NSI parameter is clearly broken, and now we have two separate intervals at a 90% CL. Another optimistic scenario is given in case 4, where both the mass and threshold are significantly improved with respect to case 1. Finally, in case 5, we study the impact of an even lower threshold of 210 keV_{ee}, as reported by the CONUS Collaboration in Ref. [70], from where we have also extracted the background model for the additional bins. We can clearly see from the figure that the best sensitivity is achieved in this last scenario. In the right panel in the figure, we show the corresponding results for the flavor-changing NSI parameter $\epsilon_{e\tau}^{dV}$. As expected, improving either the mass or threshold of the detector results in a better sensitivity, getting again the best expected constraint for case 5.

As a second experimental scenario, we consider a νGeN -like detector, with the same characteristics and background model as in Ref. [39]. The sensitivity to neutrino NSIs in this case is presented in Fig. 8. As before, solid pink lines represent the expected sensitivity for a detector with the same characteristics described in Sec. III and labeled as case 1. The other lines in the figure correspond to more optimistic scenarios that result from either increasing the detector mass or broadening the region of interest in nuclear

recoil energy (indicated as the yellow region in the right panel in Fig. 3) with respect to case 1. The different experimental setups under consideration are listed in Table II. Qualitatively, we see that these results are similar to the case of the CONUS-like detector.

D. Constraining neutron rms radius and NSIs simultaneously

After analyzing nuclear effects and NSIs individually, we now proceed to test these two physical cases simultaneously at π -DAR sources. The motivation behind this analysis lies in the fact that the uncertainties in nuclear form factors and the presence of neutrino NSIs with matter might be confused in a π -DAR experiment. Thus, a discrepancy between the predicted and the observed signal in this type of experiment could be interpreted in terms of one of these hypotheses or even the combination of the two of them. Interestingly, the joint analysis with CE ν NS searches at reactor experiments, not sensitive to nuclear uncertainties, might help to lift the degeneracy between the two scenarios and improve the determination of nuclear and NSI parameters.

We start by analyzing the currently available COHERENT CsI data, allowing simultaneously for different values of the neutron rms radius R_n and the presence of neutrino nonstandard interactions with matter. The analysis follows the strategy presented in Sec. IV. Differently to the individual analysis in Secs. VA and VB, here we evaluate the χ^2 function in Eq. (18) varying at the same time the set of parameters $X = \{R_n, \epsilon_{\alpha\beta}^{qV}\}$.⁸ The results of our analysis are presented in Fig. 9. Colored areas in the top panels show the allowed regions in the plane $(R_n, \epsilon_{ee}^{dV})$ in the left panel, $(R_n, \epsilon_{ee}^{uV})$ in the central panel, and $(R_n, \epsilon_{e\tau}^{dV})$ in the right panel. The pink regions show the results at 90% CL for two degrees of freedom. Notice that the presence of nonuniversal NSIs allows for values of the neutron rms radius as low as ≈ 4.2 fm, while in the case of the flavor-changing NSIs, the rms radius is bounded from below at ≈ 4.7 fm. This can be understood by considering that, when fitting the data, the presence of flavor-changing NSIs always increases the expected number of events, while nonuniversal NSIs interfere with the SM prediction and may increase or reduce the number of expected events. As a result, the value of R_n is less constrained in the latter case. For completeness, the colored blue regions in the figure show the results at the 1σ level.

In general, from the colored regions in Fig. 9, we can see that SNS data alone are not very sensitive to constrain nuclear parameters when simultaneously considering NSI effects. Therefore, in this section we are going to investigate whether the combination with results obtained with

⁸A similar analysis on the parameter space $(R_n, \epsilon_{ee}^{dV})$ using the 2017 COHERENT CsI dataset was performed in Ref. [42].

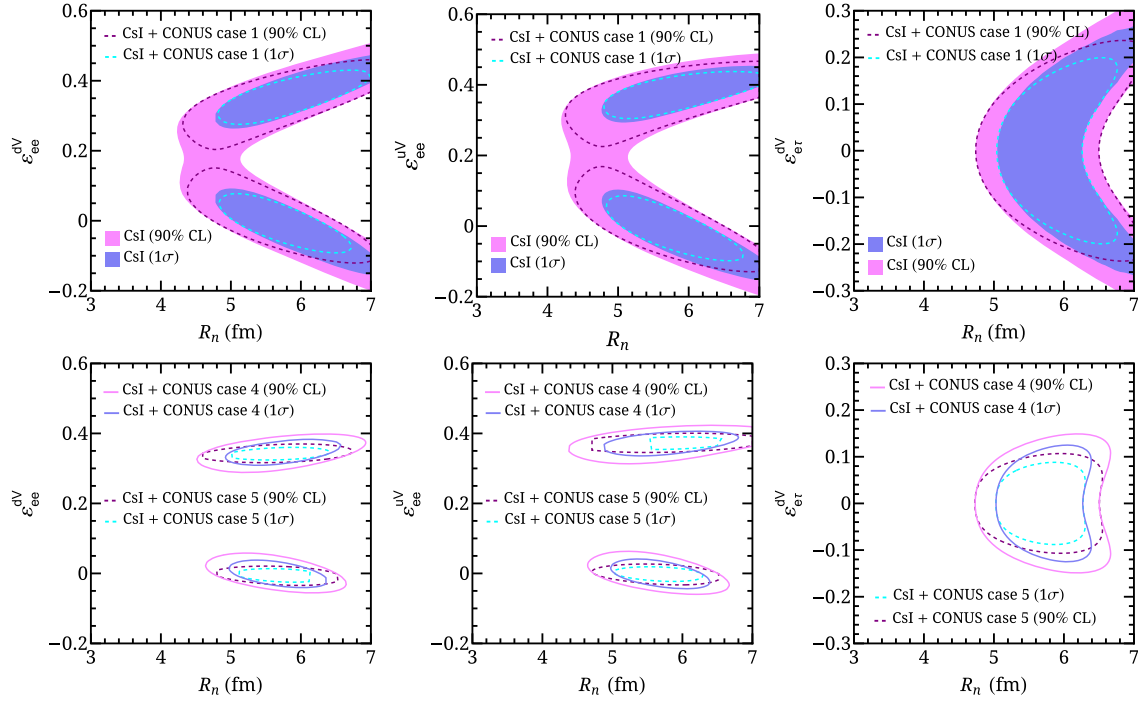


FIG. 9. Top panels: Colored areas indicate the expected 1σ (blue) and 90% CL (pink) allowed regions from current CsI COHERENT data in the $(R_n, \epsilon_{ee}^{dV})$, $(R_n, \epsilon_{ee}^{uV})$, and $(R_n, \epsilon_{e\tau}^{dV})$ planes. Dashed contours correspond to the combination with the case 1 CONUS-like reactor experiment setup at 1σ (blue lines) and 90% CL (black lines). Bottom panels: 1σ and 90% CL allowed regions from the combination of CsI data and the scenarios 4 (solid line) and 5 (dashed line) presented in Table II.

different neutrino sources can improve the sensitivity to these parameters. We combine the previous CsI results with the expected sensitivity of the reactor experiments described in the previous section to neutrino NSIs. As a particular example, we combine COHERENT data with the CONUS-like reactor experiment studied above. Regions enclosed by dashed lines in the top panels in Fig. 9 show the results from the combination of CsI data and the CONUS-like detector with the experimental characteristics labeled as case 1 in Table II. Again, the pink color corresponds to 90% CL and the blue color to 1σ level. For the latter, one sees that, in all three panels, the combination results in a closed region around the SM solution. Additionally, the bottom panels of the same figure explore the combination of the results assuming the more futuristic reactor scenarios indicated as case 4 (solid lines) and case 5 (dashed lines) in Table II. Notice that, even at 90% CL, and in both cases 4 and 5, we obtain closed regions in the parameter space in the three panels, making the determination of the neutron rms radius in the presence of NSIs more robust from the combination of the two types of neutrino sources.

After trying to simultaneously constrain the neutron rms radius and neutrino NSIs with current accelerator data, we now consider the expected sensitivity of the future π -DAR source detectors discussed in Sec. III by minimizing the χ^2 function defined in Eq. (20). The expected results assuming

a ^{72}Ge detector at the SNS are shown in the top panels in Fig. 10 as blue (1σ) and pink regions (90% CL) in the planes $(R_n, \epsilon_{ee}^{dV})$ in the left panel, $(R_n, \epsilon_{ee}^{uV})$ in the central panel, and $(R_n, \epsilon_{e\tau}^{dV})$ in the right panel. For nonuniversal NSIs, we can clearly see the presence of two separate regions, one around the SM model prediction and another one preferring nonzero values for the NSIs and, therefore, allowing for larger values of the neutron rms radius. The results for flavor-changing NSIs with down quarks in the right panel show that, the more $\epsilon_{e\tau}^{dV}$ deviates from zero, the larger the allowed value for R_n . The corresponding results for flavor-changing NSIs with up quarks are very similar, and we do not show them here.

As in the case of CsI, we now proceed to analyze the combined sensitivity of the future Ge detector at the SNS described in Table I with our forecast for NSI searches at upcoming CE ν NS searches at reactor experiments. Contours surrounded by dashed lines in the top panels in Fig. 10 show the combination with the CONUS-like case 1 indicated in Table II. Since for this case the reactor NSI constraints are not competitive, the allowed region in each panel remains almost unchanged and the complementarity between the two experiments is not evident. The situation is different when we combine the SNS analysis with the most optimistic CONUS-like cases 4 and 5, listed in Table II, as seen from the solid and dashed lines in the bottom panels in Fig. 10. Here, the improvement obtained with the combined

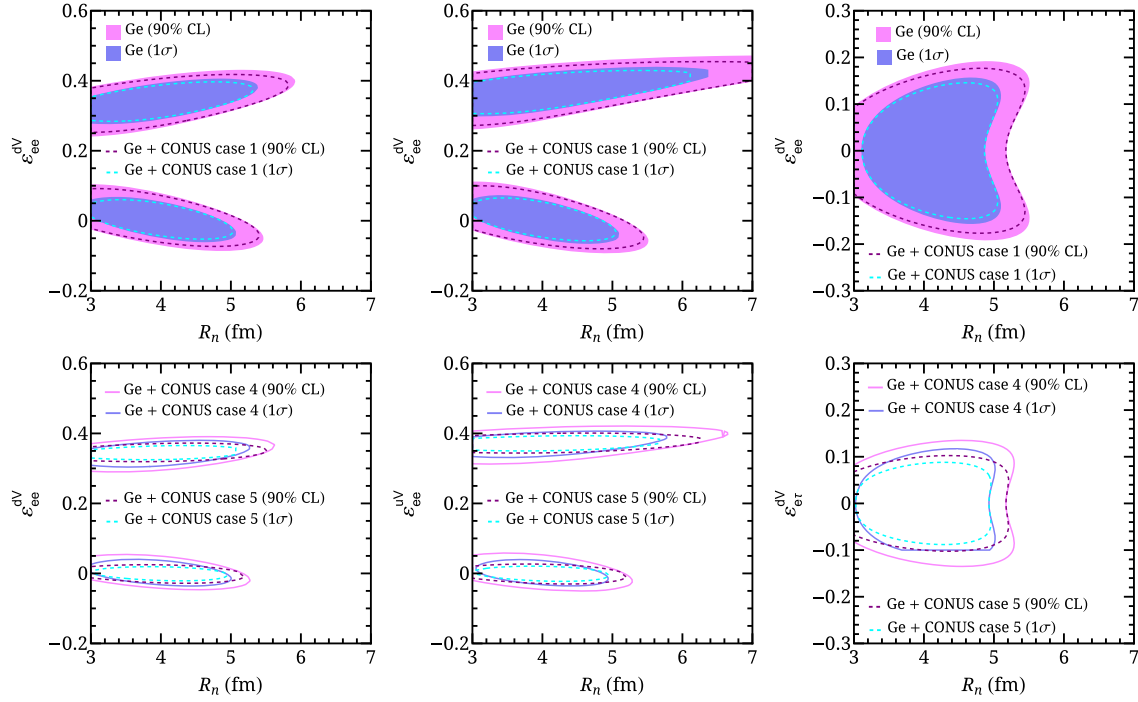


FIG. 10. Top panels: Colored areas indicate the expected 1σ (blue) and 90% CL (pink) allowed regions from a future Ge detector at the SNS in the $(R_n, \epsilon_{cc}^{dV})$, $(R_n, \epsilon_{cc}^{uV})$, and $(R_n, \epsilon_{\epsilon\tau}^{dV})$ planes. Dashed contours correspond to the combination with the case 1 CONUS-like reactor experiment setup at 1σ (blue lines) and 90% CL (black lines). Bottom panels: 1σ and 90% CL allowed regions from the combination of the Ge detector at the SNS and the cases 4 (solid line) and 5 (dashed line) presented in Table II.

analysis is clearly seen in the three panels, where the allowed region of R_n is reduced and the sensitivity to the NSI couplings is dominated by reactor data.

To conclude this section, we present the joint analysis of the future Xe detector at the ESS described in Table I and a future ν GeN-like reactor detector. The results for the π -DAR Xe detector alone are displayed as colored regions in the top panels in Fig. 11, with the same color code as in previous figures, for ϵ_{cc}^{dV} (left), ϵ_{cc}^{uV} (central), and $\epsilon_{\epsilon\tau}^{dV}$ (right). Dashed lines in the same panels show the results of the combined analysis from a Xe detector with a CE ν NS reactor neutrino experiment ν GeN-like detector, as described in Sec. III and in case 1 in Table II. The combination with cases 4 and 5 is presented in the bottom panels of the figure with solid and dashed lines, respectively. Note that the results presented in Figs. 10 and 11 are not directly comparable, since the chosen target materials at the SNS and ESS are different. However, we see some qualitative similarities between the two analyses, showing the complementarity between the CE ν NS measurements from different neutrino sources.

In the examples above, we have shown how combining experiments with different sources can help to constrain the neutron rms radius and, hence, complement the current list of measured neutron rms radii [49], in the presence of NSIs. However, considering the theoretical uncertainties discussed in Sec. II and comparing our results with the

experimental sensitivities achieved for other nuclei [49], a better sensitivity from our analysis would be desirable. To this end, in the next subsection, we will discuss how the sensitivity on the neutron rms radius from CE ν NS can eventually be improved by collecting more statistics on the Ge detectors at the SNS.

E. Constraining neutron rms radius with improved statistics

The results presented so far show the complementarity between reactor and accelerator CE ν NS data to constrain nuclear physics and NSI effects. As we have seen, the combination of the considered experimental setups can constrain significantly the parameter space, but, unfortunately, it cannot reach competitive sensitivities for the neutron rms radius. In this section, we try to find out if the same experiments with larger statistics can contribute to obtain a better sensitivity on this parameter. To illustrate this, we redo our previous analysis, considering a scenario with longer running time for both spallation sources and reactor CE ν NS experiments. The results of this reanalysis are presented in Fig. 12. The magenta regions in the left panel show the expected 90% CL sensitivity obtained considering 5 years of data taking in our germanium detector model at the SNS alone, while the dashed contours correspond to the improved sensitivity obtained after combining with the analysis of case 5 CONUS-like

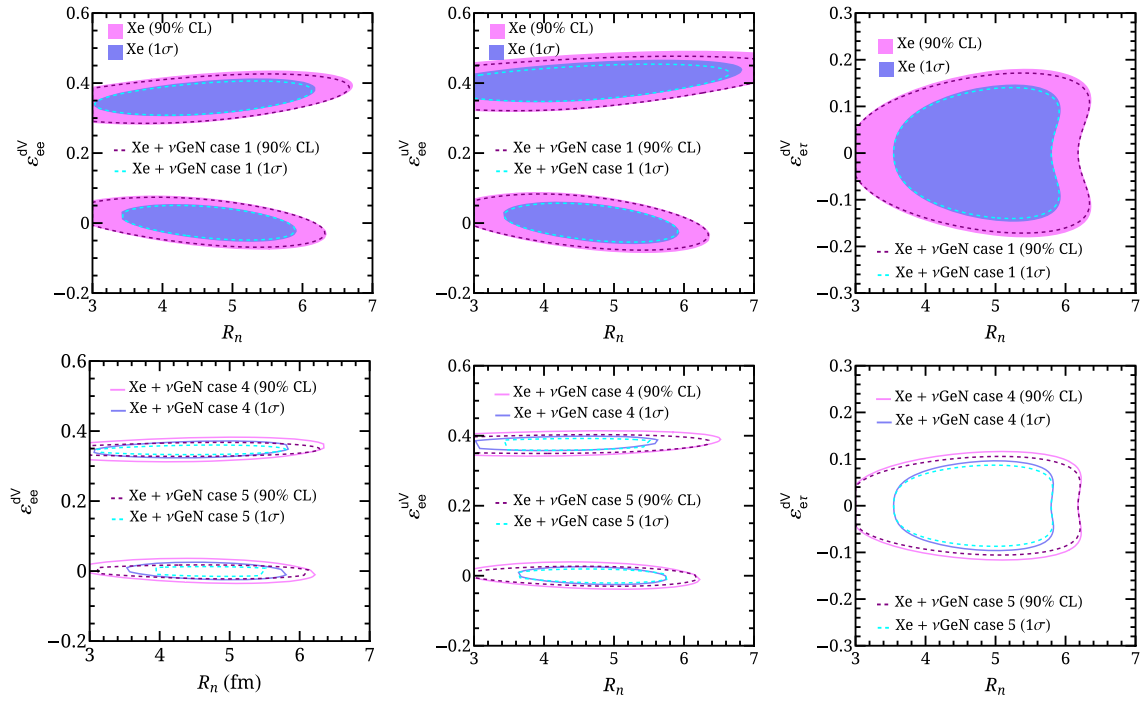


FIG. 11. Top panels: Colored areas indicate the expected 1σ (blue) and 90% CL (pink) allowed regions from a Xe detector at the ESS in the $(R_n, \epsilon_{ee}^{dV})$, $(R_n, \epsilon_{ee}^{uV})$, and $(R_n, \epsilon_{ee}^{dV})$ planes. Dashed contours correspond to the combination with the case ν GeN-like reactor experiment setup at 1σ (blue lines) and 90% CL (black lines). Bottom panels: 1σ and 90% CL allowed regions from the combination of the Xe detector at the ESS and the cases 4 (solid line) and 5 (dashed line) presented in Table II.

experimental setup defined in Table II but after a running period of 5 years. In this case, the neutron rms radius is constrained to $R_n \in (3.17, 4.85)$ fm at 90% CL when NSI interactions are also allowed. Our result can be further improved if we double the detector mass of the germanium SNS-like detector from 16 to 32 kg, which would be equivalent to running the experiment for 10 years. The results of this analysis alone are shown as magenta regions in the right panel in Fig. 12, while the combined analysis with a 5-year CONUS-like detector is shown as the dashed

contour. Under these conditions, the neutron rms radius would be constrained to $R_n \in (3.43, 4.66)$ fm at 90% CL when allowing for NSI interactions, a result that begins to be competitive with different computations of the neutron rms radius, as discussed at the end of Sec. II A. Let us remark that, while the results presented in the previous section show the information one can extract by combining data from different sources at CE ν NS experiments under a conservative approach, the (perhaps too optimistic) assumptions considered here illustrate how sensitive experiments can be with high enough statistics.

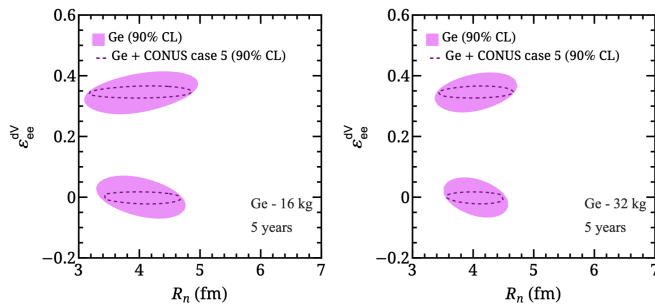


FIG. 12. Left panel: Magenta regions show the 90% CL sensitivity to $(R_n, \epsilon_{ee}^{dV})$ that a 16 kg germanium detector can reach after 5 years of data taking at the SNS. Dashed contours show the result after combining with 5 years of data of a CONUS-like detector under the conditions listed as case 5 in Table II. Right panel: the same as in the left panel but considering 32 kg for the germanium detector at the SNS.

VI. CONCLUSIONS

In this paper, we have studied the complementarity between CE ν NS experiments that use different neutrino sources as well as various detection target materials to constrain nuclear uncertainties and new neutrino interactions with matter. Besides analyzing the sensitivity of current and future experimental setups to these physics cases individually, one of the main goals of this work consists of showing the synergies between CE ν NS experiments with π -DAR and reactor neutrino sources to simultaneously constrain the two scenarios. This analysis is motivated by the fact that, at CE ν NS experiments with π -DAR sources, nuclear uncertainties parametrized in the neutron rms radius and neutrino NSIs would produce a similar impact on the observed neutrino signal. As a result,

it would be impossible to disentangle the origin of a potential deviation with respect to the SM predicted signal, and the sensitivity to new physics beyond the SM would be strongly affected by that. Indeed, we have shown that, when analyzing data from stopped pion sources alone, the presence of nuclear uncertainties relevant for the CE ν NS cross section might allow for rather large values of neutrino NSI couplings. Fortunately, combined analyses of π -DAR data with reactor CE ν NS experiments, insensitive to nuclear uncertainties, can help break this degeneracy and, thus, provide more constraining results.

In our analysis, we have first estimated the sensitivity of stopped pion CE ν NS experiments to nuclear physics and nonstandard neutrino interactions separately, as well as the potential of CE ν NS reactor neutrino experiments to constrain NSIs. As for π -DAR experiments, we have considered the latest data from the CsI COHERENT experiment, the expected signal at the Ge COHERENT detector at the SNS, and a potential experiment using a Xe detector at the ESS. In the reactor sector, we have proposed two experimental configurations based on optimized versions of the existing detectors CONUS and ν GeN. We have also estimated the sensitivity of π -DAR experiments to the two physics cases simultaneously, showing the presence of a degeneracy between R_n and neutrino NSIs with matter, for both nonuniversal and flavor-changing interactions. This degeneracy is particularly relevant in the case of current CsI COHERENT data, although it also affects the sensitivity of the Ge detector at the SNS and a potential Xe detector at the ESS. Even though the combination with the

near-future sensitivity of a CONUS-like CE ν NS reactor experiment can only slightly improve the sensitivity to the neutron rms radius, we have shown that a further improvement in the mass and threshold of the detector in a CONUS-like reactor experiment can have a significant impact on the determination of the neutron rms radius and the size of the NSI couplings. This illustrates the complementarity of CE ν NS experiments using different neutrino sources to constrain the presence of new physics beyond the SM, even in the presence of nuclear uncertainties that could hinder this task. The choice of potential future experiments in this work is mainly based on the optimization of existing CE ν NS experiments and could be regarded as a guide to enhance the experimental sensitivity to new physics in the presence of nuclear uncertainties.

ACKNOWLEDGMENTS

We thank Dimitris Papoulias, Omar Miranda, and Luis Alvarez-Ruso for very fruitful discussions. This work was supported by the Spanish Grants No. PID2020–113775GB-I00 (MCIN/AEI/10.13039/501100011033), No. CIPROM/2021/054. G. S. G. acknowledges financial support by the Grant No. CIAPOS/2022/254 (Generalitat Valenciana). M. T. is also supported by Fundação para a Ciência e a Tecnologia (FCT, Portugal) through Project No. CERN/FIS-PAR/0019/2021. R. R. R. has received support from the Coordenação de Aperfeiçoamento de Pessoal de Nível Superior—Brasil (CAPES)—Finance Code 001.

-
- [1] D. Z. Freedman, Coherent effects of a weak neutral current, *Phys. Rev. D* **9**, 1389 (1974).
 - [2] D. Akimov *et al.*, Observation of coherent elastic neutrino-nucleus scattering, *Science* **357**, 1123 (2017).
 - [3] D. Akimov *et al.*, First measurement of coherent elastic neutrino-nucleus scattering on argon, *Phys. Rev. Lett.* **126**, 012002 (2021).
 - [4] D. Akimov *et al.*, Measurement of the coherent elastic neutrino-nucleus scattering cross section on CsI by COHERENT, *Phys. Rev. Lett.* **129**, 081801 (2022).
 - [5] M. Atzori Corona, M. Cadeddu, N. Cargioli, F. Dordei, C. Giunti, and G. Masia, Nuclear neutron radius and weak mixing angle measurements from latest COHERENT CsI and atomic parity violation Cs data, *Eur. Phys. J. C* **83**, 683 (2023).
 - [6] M. Cadeddu, N. Cargioli, F. Dordei, C. Giunti, Y. F. Li, E. Picciau, C. A. Ternes, and Y. Y. Zhang, New insights into nuclear physics and weak mixing angle using electroweak probes, *Phys. Rev. C* **104**, 065502 (2021).
 - [7] M. Cadeddu, C. Giunti, Y. F. Li, and Y. Y. Zhang, Average CsI neutron density distribution from COHERENT data, *Phys. Rev. Lett.* **120**, 072501 (2018).
 - [8] D. K. Papoulias, T. S. Kosmas, R. Sahu, V. K. B. Kota, and M. Hota, Constraining nuclear physics parameters with current and future COHERENT data, *Phys. Lett. B* **800**, 135133 (2020).
 - [9] T. Ohlsson, Status of non-standard neutrino interactions, *Rep. Prog. Phys.* **76**, 044201 (2013).
 - [10] P. B. Denton and J. Gehrlein, A statistical analysis of the COHERENT data and applications to new physics, *J. High Energy Phys.* **04** (2021) 266.
 - [11] O. G. Miranda, D. K. Papoulias, G. Sanchez Garcia, O. Sanders, M. Tórtola, and J. W. F. Valle, Implications of the first detection of coherent elastic neutrino-nucleus scattering (CE ν NS) with Liquid Argon, *J. High Energy Phys.* **05** (2020) 130; **01** (2021) 67.
 - [12] C. Giunti, General COHERENT constraints on neutrino nonstandard interactions, *Phys. Rev. D* **101**, 035039 (2020).
 - [13] O. G. Miranda, G. Sanchez Garcia, and O. Sanders, Coherent elastic neutrino-nucleus scattering as a precision test for the standard model and beyond: The COHERENT proposal case, *Adv. High Energy Phys.* **2019**, 3902819 (2019); **2022**, 9874517(E) (2022).

- [14] O. G. Miranda, D. K. Papoulias, M. Tórtola, and J. W. F. Valle, Probing neutrino transition magnetic moments with coherent elastic neutrino-nucleus scattering, *J. High Energy Phys.* **07** (2019) 103.
- [15] T. S. Kosmas, O. G. Miranda, D. K. Papoulias, M. Tortola, and J. W. F. Valle, Probing neutrino magnetic moments at the Spallation Neutron Source facility, *Phys. Rev. D* **92**, 013011 (2015).
- [16] M. Cadeddu, C. Giunti, K. A. Kouzakov, Y.-F. Li, Y.-Y. Zhang, and A. I. Studenikin, Neutrino charge radii from coherent elastic neutrino-nucleus scattering, *Phys. Rev. D* **98**, 113010 (2018); **101**, 059902(E) (2020).
- [17] A. Parada, Constraints on neutrino electric millicharge from experiments of elastic neutrino-electron interaction and future experimental proposals involving coherent elastic neutrino-nucleus scattering, *Adv. High Energy Phys.* **2020**, 5908904 (2020).
- [18] M. Lindner, W. Rodejohann, and X.-J. Xu, Coherent neutrino-nucleus scattering and new neutrino interactions, *J. High Energy Phys.* **03** (2017) 097.
- [19] D. Aristizabal Sierra, V. De Romeri, and N. Rojas, COHERENT analysis of neutrino generalized interactions, *Phys. Rev. D* **98**, 075018 (2018).
- [20] L. J. Flores, N. Nath, and E. Peinado, CE ν NS as a probe of flavored generalized neutrino interactions, *Phys. Rev. D* **105**, 055010 (2022).
- [21] D. Aristizabal Sierra, V. De Romeri, and N. Rojas, CP violating effects in coherent elastic neutrino-nucleus scattering processes, *J. High Energy Phys.* **09** (2019) 069.
- [22] M. Abdullah, J. B. Dent, B. Dutta, G. L. Kane, S. Liao, and L. E. Strigari, Coherent elastic neutrino nucleus scattering as a probe of a Z' through kinetic and mass mixing effects, *Phys. Rev. D* **98**, 015005 (2018).
- [23] M. Cadeddu, N. Cargioli, F. Dordei, C. Giunti, Y. F. Li, E. Picciau, and Y. Y. Zhang, Constraints on light vector mediators through coherent elastic neutrino nucleus scattering data from COHERENT, *J. High Energy Phys.* **01** (2021) 116.
- [24] L. J. Flores, N. Nath, and E. Peinado, Non-standard neutrino interactions in U(1)' model after COHERENT data, *J. High Energy Phys.* **06** (2020) 045.
- [25] T. S. Kosmas, D. K. Papoulias, M. Tortola, and J. W. F. Valle, Probing light sterile neutrino signatures at reactor and Spallation Neutron Source neutrino experiments, *Phys. Rev. D* **96**, 063013 (2017).
- [26] C. Blanco, D. Hooper, and P. Machado, Constraining sterile neutrino interpretations of the LSND and MiniBooNE anomalies with coherent neutrino scattering experiments, *Phys. Rev. D* **101**, 075051 (2020).
- [27] P. M. Candela, V. De Romeri, and D. K. Papoulias, COHERENT production of a Dark Fermion, *Phys. Rev. D* **108**, 055001 (2023).
- [28] V. De Romeri, O. G. Miranda, D. K. Papoulias, G. Sanchez Garcia, M. Tórtola, and J. W. F. Valle, Physics implications of a combined analysis of COHERENT CsI and LAr data, *J. High Energy Phys.* **04** (2023) 035.
- [29] D. Akimov *et al.*, Simulating the neutrino flux from the Spallation Neutron Source for the COHERENT experiment, *Phys. Rev. D* **106**, 032003 (2022).
- [30] A. A. Aguilar-Arevalo *et al.*, First dark matter search results from Coherent CAPTAIN-Mills, *Phys. Rev. D* **106**, 012001 (2022).
- [31] D. Baxter *et al.*, Coherent elastic neutrino-nucleus scattering at the European spallation source, *J. High Energy Phys.* **02** (2020) 123.
- [32] D. Akimov *et al.*, The COHERENT experimental program, [arXiv:2204.04575](https://arxiv.org/abs/2204.04575).
- [33] P. S. Barbeau *et al.*, Accessing new physics with an undoped, cryogenic CsI CEvNS detector for COHERENT at the SNS, 11 2023.
- [34] A. Galindo-Uribarri, O. G. Miranda, and G. S. Garcia, Novel approach for the study of coherent elastic neutrino-nucleus scattering, *Phys. Rev. D* **105**, 033001 (2022).
- [35] S. S. Chatterjee, S. Lavignac, O. Miranda, and G. S. Garcia, Constraining nonstandard interactions with coherent elastic neutrino-nucleus scattering at the European spallation source, *Phys. Rev. D* **107**, 055019 (2023).
- [36] C. von Raesfeld and P. Huber, Use of CEvNS to monitor spent nuclear fuel, *Phys. Rev. D* **105**, 056002 (2022).
- [37] J. Colaresi, J. I. Collar, T. W. Hossbach, C. M. Lewis, and K. M. Yocum, Measurement of coherent elastic neutrino-nucleus scattering from reactor antineutrinos, *Phys. Rev. Lett.* **129**, 211802 (2022).
- [38] H. Bonet *et al.*, Constraints on elastic neutrino nucleus scattering in the fully coherent regime from the CONUS experiment, *Phys. Rev. Lett.* **126**, 041804 (2021).
- [39] I. Alekseev *et al.*, First results of the ν GeN experiment on coherent elastic neutrino-nucleus scattering, *Phys. Rev. D* **106**, L051101 (2022).
- [40] A. Aguilar-Arevalo *et al.*, Search for coherent elastic neutrino-nucleus scattering at a nuclear reactor with CONNIE 2019 data, *J. High Energy Phys.* **05** (2022) 017.
- [41] D. Y. Akimov *et al.*, The RED-100 experiment, *J. Instrum.* **17**, T11011 (2022).
- [42] B. Canas, E. Garces, O. Miranda, A. Parada, and G. S. Garcia, Interplay between nonstandard and nuclear constraints in coherent elastic neutrino-nucleus scattering experiments, *Phys. Rev. D* **101**, 035012 (2020).
- [43] O. Tomalak, P. Machado, V. Pandey, and R. Plestid, Flavor-dependent radiative corrections in coherent elastic neutrino-nucleus scattering, *J. High Energy Phys.* **02** (2021) 097.
- [44] J. Piekarewicz, A. R. Linero, P. Giuliani, and E. Chicken, Power of two: Assessing the impact of a second measurement of the weak-charge form factor of ^{208}Pb , *Phys. Rev. C* **94**, 034316 (2016).
- [45] R. H. Helm, Inelastic and elastic scattering of 187-MeV electrons from selected even-even nuclei, *Phys. Rev.* **104**, 1466 (1956).
- [46] S. R. Klein and J. Nystrand, Exclusive vector meson production in relativistic heavy ion collisions, *Phys. Rev. C* **60**, 014903 (1999).
- [47] D. A. Sierra, Extraction of neutron density distributions from high-statistics coherent elastic neutrino-nucleus scattering data, *Phys. Lett. B* **845**, 138140 (2023).
- [48] I. Angeli and K. P. Marinova, Table of experimental nuclear ground state charge radii: An update, *At. Data Nucl. Data Tables* **99**, 69 (2013).

- [49] A. Trzcinska, J. Jastrzebski, P. Lubinski, F. J. Hartmann, R. Schmidt, T. von Egidy, and B. Klos, Neutron density distributions deduced from anti-protonic atoms, *Phys. Rev. Lett.* **87**, 082501 (2001).
- [50] C.G. Payne, S. Bacca, G. Hagen, W. Jiang, and T. Papenbrock, Coherent elastic neutrino-nucleus scattering on ^{40}Ar from first principles, *Phys. Rev. C* **100**, 061304 (2019).
- [51] M. Hoferichter, J. Menéndez, and A. Schwenk, Coherent elastic neutrino-nucleus scattering: EFT analysis and nuclear responses, *Phys. Rev. D* **102**, 074018 (2020).
- [52] D. Adhikari *et al.*, Accurate determination of the neutron skin thickness of ^{208}Pb through parity-violation in electron scattering, *Phys. Rev. Lett.* **126**, 172502 (2021).
- [53] D. Adhikari *et al.*, Precision determination of the neutral weak form factor of $\text{Ca}48$, *Phys. Rev. Lett.* **129**, 042501 (2022).
- [54] L. Wolfenstein, Neutrino oscillations in matter, *Phys. Rev. D* **17**, 2369 (1978).
- [55] J. Barranco, O. G. Miranda, and T. I. Rashba, Probing new physics with coherent neutrino scattering off nuclei, *J. High Energy Phys.* **12** (2005) 021.
- [56] Y. Farzan and M. Tortola, Neutrino oscillations and non-standard interactions, *Front. Phys.* **6**, 10 (2018).
- [57] E. Picciau, Low-energy signatures in DarkSide-50 experiment and neutrino scattering processes, Ph.D. thesis, Cagliari University, 2022.
- [58] K. Mann, Measuring coherent neutrino scattering with Ge, <https://indico.fnal.gov/event/19348/contributions/186707/>, 2020 [accessed 23-Jun-2023].
- [59] H. Abele *et al.*, Particle Physics at the European Spallation Source, *Phys. Rep.* **1023**, 1 (2023).
- [60] V. I. Kopeikin, Flux and spectrum of reactor antineutrinos, *Phys. At. Nucl.* **75**, 143 (2012).
- [61] P. Huber, Determination of antineutrino spectra from nuclear reactors, *Phys. Rev. C* **84**, 024617 (2011).
- [62] T. A. Mueller *et al.*, Improved predictions of reactor antineutrino spectra, *Phys. Rev. C* **83**, 054615 (2011).
- [63] V. Kopeikin, L. Mikaelyan, and V. Sinev, Reactor as a source of antineutrinos: Thermal fission energy, *Phys. At. Nucl.* **67**, 1892 (2004).
- [64] C. Buck *et al.*, A novel experiment for coherent elastic neutrino nucleus scattering: CONUS, *J. Phys. Conf. Ser.* **1342**, 012094 (2020).
- [65] E. Sanchez, The conus+ experiment, <https://indi.to/TRz9Z>, 2023 [accessed 13-Oct-2023].
- [66] H. Bonet *et al.*, Novel constraints on neutrino physics beyond the standard model from the CONUS experiment, *J. High Energy Phys.* **05** (2022) 085.
- [67] D. Pershey, New results from the coherent csi[na] detector, *Talk at Magnificent Cevns* (2020), <https://indico.cern.ch/event/943069/contributions/4066386/>.
- [68] C. J. Horowitz *et al.*, Weak charge form factor and radius of ^{208}Pb through parity violation in electron scattering, *Phys. Rev. C* **85**, 032501 (2012).
- [69] P. Coloma, I. Esteban, M.C. Gonzalez-Garcia, L. Larizgoitia, F. Monrabal, and S. Palomares-Ruiz, Bounds on new physics with data of the Dresden-II reactor experiment and COHERENT, *J. High Energy Phys.* **05** (2022) 037.
- [70] N. Ackermann *et al.*, Final CONUS results on coherent elastic neutrino nucleus scattering at the Brokdorf reactor, [arXiv:2401.07684](https://arxiv.org/abs/2401.07684).